Tests of Fundamental Physics

29

Eite Tiesinga and Peter J. Mohr

Contents

Abstract

We describe recent developments in tests of quantum electrodynamics (QED), the theory of the interactions of matter with electromagnetic fields. The tests focus on consistency in the determination of parameters or constants within QED obtained via multiple independent means and, in particular, by comparisons of precision measurements with equivalently accurate theoretical calculations. The most precise tests rely on a combination of the spectroscopy of atomic hydrogen, g-factor measurements of a free electron as well as that of an electron bound in a hydrogen-like ion, and finally the mass determination of the ions through atom recoil experiments and mass spectrometry. These experiments determine the dimensionless fine-structure constant and the mass of the electron to about ten significant digits, orders of magnitude better than any other description of nature. We also show that an international system of units (SI) based on fixed values of the Planck constant and the charge of the electron (in addition to the fixed value of the speed of light in vacuum) modifies the interpretation of some of these tests.

Keywords

fundamental constants · quantum electrodynamics · g-factors · proton radius puzzle · hydrogen energy levels

E. Tiesinga (✉)
National Institute of Standards and Technology
Gaithersburg, MD, USA
e-mail: eite.tiesinga@nist.gov

P. J. Mohr
National Institute of Standards and Technology
Gaithersburg, MD, USA
e-mail: mohr@nist.gov

29.1 Introduction

Tests of the fundamental laws of nature are crucial for the foundations of our knowledge of physics. The most precise theory is quantum electrodynamics (QED), which describes charged particles interacting with electromagnetic fields. It is a well-verified theory with uncertainties of observables approaching a few parts in 10^{13} for the g-factor of the electron. Our ability to test the theory is still improving with no sign of a breakdown. For example, Fig. 29.1 shows that over the past 100 years the relative uncertainty of the dimensionless fine-structure constant α has seen an exponential improvement by eight orders of magnitude to a 2014 relative uncertainty of 2×10^{-10}. In some cases, the precision of the tests is now limited by our understanding of another fundamental theory, namely quantum chromodynamics (QCD). For example, nuclear-structure effects limit the comparison between theory and experiment for the hyperfine structure of hydrogen.

On May 20, 2019 the International System of Units (SI) [2] was redefined based on fixing the values of fundamental constants that appear naturally in the laws of physics. This continues a trend started in 1983 when the speed of light

G.W.F. Drake (Ed.), *Springer Handbook of Atomic, Molecular, and Optical Physics*, Springer Handbooks,
https://doi.org/10.1007/978-3-030-73893-8_29

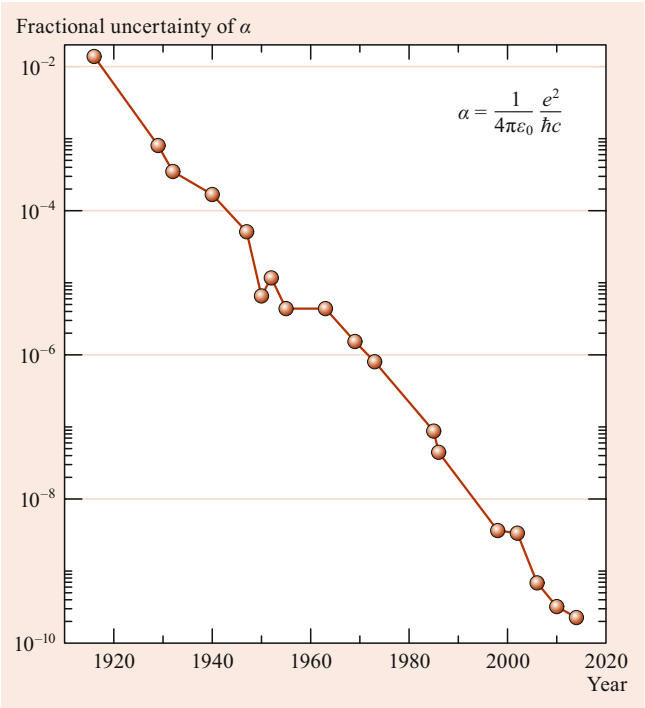

Fig. 29.1 Fractional uncertainty of the fine-structure constant α over the past 100 years, starting in 1916 with the introduction of α by *A. Sommerfeld* [1]

in vacuum, c, was fixed [3]. Now the reduced Planck constant $\hbar$, electron charge e, the Boltzmann constant k, and the Avogadro constant N_A have also been fixed. Although the laws of nature are independent of the definitions of the units, the transition to the revised SI does change our perspective on the tests.

This chapter reviews comparisons between theory and experiment that test our understanding of laws of nature. The focus is on quantitative tests of QED through measurements of hydrogen energy levels, the g-factors of the electron and hydrogen-like ions, and atom recoil energies from photon interactions. These measurements determine the fine-structure constant α, the electron mass m_e, and atomic masses, and demonstrate consistency of the theory. It is worth noting that the dimensionless constant $\alpha \equiv e^2/(4\pi\epsilon_0\hbar c)$ is much less than one, where ϵ_0 is the electric constant or permittivity of vacuum. Recent reviews that cover topics in this chapter are given in [4, 5]. Our values of inexactly-known fundamental constants are the 2014 CODATA recommended values [5], unless otherwise noted.

29.2 Consistency of Fundamental Physics

The most precise tests of quantum electrodynamics are intertwined with the determination of the fine-structure constant, electron mass, and masses of atoms. In fact, the measurements are determinations of transition frequencies in hydrogen, spin-flip and cyclotron frequencies of the free and bound electron in a magnetic field, as well as atom recoil energies. They are compared to theoretical expressions for these observables, which, generally, are functions of fundamental constants.

For a hydrogen atom at rest, the energy of state i is

$$E_i = (m_p + m_e)c^2 - \frac{1}{2}m_e c^2\alpha^2\left\{\frac{1}{n_i^2} + \cdots\right\}, \qquad (29.1)$$

where m_p is the mass of the proton, and n_i is the principal quantum number of state i. It will be convenient to use the Hartree energy $E_h = m_e c^2\alpha^2$. The dots in this theoretical expression indicate corrections that are small compared to the leading term. Examples are contributions that are higher-order in α, of order of the electron–proton mass ratio m_e/m_p, and of order of the ratio of the root-mean-square (rms) proton charge radius to the Bohr radius r_p/a_0. Equation (29.1) also sets the mass of the hydrogen atom in state i, that is, $m(H_i) = E_i/c^2$.

Many (angular) transition frequencies

$$\omega = \frac{E_j - E_i}{\hbar} \qquad (29.2)$$

have been measured over the decades. They primarily determine the Hartree energy E_h (or equivalently the Rydberg constant R_∞.) Often the experiments, such as those measuring the energy differences between two S states, involve two-photon transitions where ω is replaced by 2ω. A second class of transitions relevant for our purposes is that where the contribution from the Bohr energies, proportional to $1/n^2$, cancels. An example is the Lamb shift between the $2P_{1/2}$ and $2S_{1/2}$ states. In this case, the transition frequencies are proportional to a higher power in α than α^2.

The frequency measurements provide a first example of the change in perspective introduced by the revised SI. In particular, in precise spectroscopy, photon frequencies ω are measured from which energy differences $\hbar\omega$ are inferred. In the SI in which $\hbar$ is not exact, this inference leads to relatively inaccurate energies in units of joules. In the revised SI, there is no loss of accuracy in this conversion.

The second ingredient for our tests of QED is a measurement of the anomaly a_e of the g-factor of the free electron placed in a homogeneous magnetic field $\vec{B}$ [6]. The electron undergoes cyclotron motion with angular frequency

$$\omega_c = 2\frac{\mu_B}{\hbar}B \qquad (29.3)$$

and spin-flip transitions with frequency

$$\omega_s = |g_e|\frac{\mu_B}{\hbar}B\,, \qquad (29.4)$$

where $\mu_B = e\hbar/(2m_e)$ is the Bohr magneton, and the electron g-factor is $g_e = -2[1 + a_e(\alpha, \ldots)]$. The anomaly is then extracted from a direct measurement of the difference of the spin-flip and cyclotron frequencies, $\omega_s - \omega_c$ and a measurement of ω_c. That is,

$$\left.\frac{\omega_s - \omega_c}{\omega_c}\right|_{\text{exp}} = a_e(\alpha, \ldots) = \frac{1}{2}\frac{\alpha}{\pi} + \ldots \,. \tag{29.5}$$

The ... indicate small corrections of higher order in α. Additional corrections are proportional to the mass ratio m_e/m_μ for vacuum polarization corrections from virtual muon loops, for example.

The hydrogen spectroscopy is, thus, a means to determine $m_e c^2\alpha^2/\hbar$ (or equivalently $m_e\alpha^2$), while g-factor measurements of the free electron determine α. Together, the two experiments thus specify α and m_e. This, however, does not constitute a test of a fundamental theory. It only determines values of the constants. The required additional input is achieved with atom recoil measurements.

The recoil energy of a neutral atom X of mass $m(X)$ initially at rest after absorption of a photon from a laser beam with angular frequency ω_1 and subsequent (resonant) emission of a photon into a laser beam with a slightly-smaller frequency ω_2 propagating in the opposite direction is

$$E_{\text{rec}} = \hbar(\omega_1 - \omega_2) = \frac{(2\hbar k)^2}{2m(X)} + \ldots \,, \tag{29.6}$$

where the average momentum of the photons is $\hbar k$, $k = \omega/c$ and $\omega = (\omega_1 + \omega_2)/2$. The ... represent small corrections mainly due to the difference in momentum of the photons in the two laser beams. (In actual realizations, many photons are scattered from the atom in order to improve accuracy.)

Photon frequencies and their differences can be measured more accurately than any of the other parameters in Eq. (29.6). Thus, we restate this equation as

$$\left.\frac{\omega^2}{(\omega_1 - \omega_2)}\right|_{\text{exp}} = \frac{1}{2}\frac{m(X)c^2}{\hbar} + \ldots \,. \tag{29.7}$$

Hence, recoil measurements determine mass $m(X)$ in the revised SI as both c and $\hbar$ are exactly defined. In the old SI, $\hbar$ was not exact, and the experiment only measured $m(X)/\hbar$.

A measurement of atomic mass does not immediately help in testing fundamental theory. We can complete the story, illustrated in Fig. 29.2, by determining the atom-to-electron mass ratio $m(X)/m_e$ and, thus, find an independent value for the electron mass. To date this occurs in a two-step process. First, mass spectrometry of atomic ions [7, 8] measures mass ratios of low-charge-state ions of atoms X and Y. The mass ratio of the corresponding neutral atom is then accurately inferred by accounting for the appropriate number of electron masses and ionization energies.

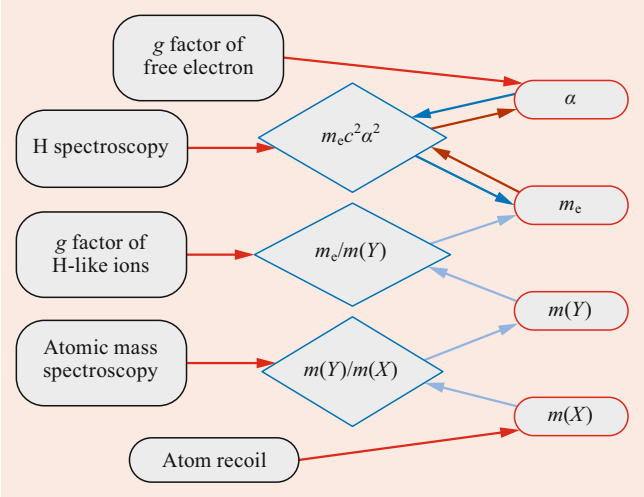

Fig. 29.2 Flow diagram for tests of QED based on the revised SI. *Black boxes* on the left-hand side correspond to the five precision experiments used to determine four fundamental constants in *red boxes* on the right-hand side. *Arrows* describe one-way connections from experiments to the constants. The constants are the fine-structure constant α, the electron mass m_e, and masses of various atoms, $m(X)$ and $m(Y)$. Most experiments only measure products or ratios of the fundamental constants shown as *blue diamonds*. For example, atomic mass spectrometry only determines ratios of atomic masses. The relations among α, m_e, and $m_e c^2\alpha^2$ can be traversed in either direction

Second, g-factor measurements of the electron bound in a hydrogen-like ion Y^{q+} determine mass ratios $m(Y^{q+})/m_e$ through spin-flip and cyclotron frequency ratios of the ion in a magnetic field and the relationship

$$\left.\frac{\omega_s(Y^{q+})}{\omega_c(Y^{q+})}\right|_{\text{exp}} = -\frac{1}{2q}\frac{m(Y^{q+})}{m_e}\, g_Y(\alpha, \ldots) \,. \tag{29.8}$$

Here, $q = Z_Y - 1$, Z_Y is the charge number of the nucleus of the ion, and the theoretical (negative) g-factor g_Y can be calculated with sufficient accuracy. The ratio $m(Y)/m_e$ is then inferred as in mass spectrometry measurements. It may seem surprising that g_Y can be calculated accurately. The key is that $g_Y \approx -2$ to lowest order in Dirac theory, and, therefore, corrections need not be computed as accurately as for the anomaly of a free electron.

This indirect approach to obtain $m(X)/m_e$ is needed as recoil experiments use atoms for which hydrogen-like g-factor measurements are not available. Moreover, mass differences between ionization stages of an atom, including those due to the binding energy of the electrons, can only be accurately accounted for in small-Z_Y ions.

The change in units from the old to the revised SI is also reflected in our understanding of mass. Figure 29.3 shows the contributions to and uncertainties of the mass of the ground-state hydrogen atom, $m(\text{H})$, in the SI unit of mass (kg) and in the atomic mass unit (amu) $m_u = m(^{12}\text{C})/12$, one twelfth of the mass of a ^{12}C atom. Clearly, the mass of the proton

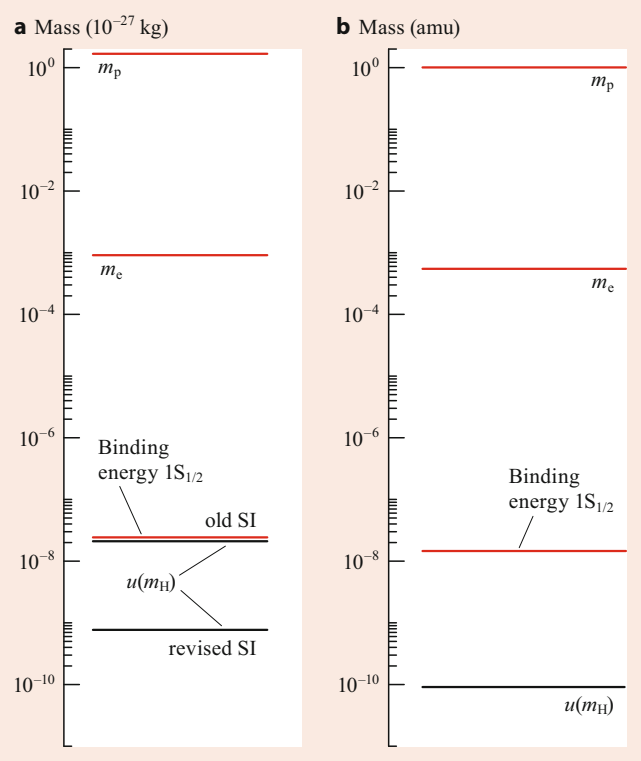

Fig. 29.3 Contributions to the mass of a $1S_{1/2}$ hydrogen atom, $m(H)$, in kilograms (**a**) and atomic mass units (**b**) on a logarithmic scale. From top to bottom, the *red lines* in each panel correspond to the mass of the proton, electron, and the absolute value of the binding energy (divided by c^2), respectively. In (**a**), the *black horizontal lines* are the uncertainties of the hydrogen mass, $u(m_H)$, in the old and revised SI. The *black line* in (**b**) shows $u(m_H)$ in atomic mass units

is by far the largest contribution and, in fact, its uncertainty fully determines the uncertainty in both units of mass. Nevertheless, in units of m_u, the hydrogen mass is known with ten significant digits as it can be relatively easily compared to the mass of a carbon atom. This has not changed in the redefinition. We also observe that in the old SI, the uncertainty of $m(H)$ in kg nearly coincides with the contribution from the binding energy. With the redefinition, the uncertainty of $m(H)$ in kg has improved by more than an order of magnitude to 1 part in 10^9 and is mainly limited by our ability to measure the fine-structure constant. This follows from expressing the hydrogen mass in terms of the atomic mass unit and that of the electron, i.e.,

$$m(\mathrm{H}) = \frac{m(\mathrm{H})}{m_u}\frac{m_u}{m_e}m_e = A_r(\mathrm{H})\frac{1}{A_r(e)}\left[\frac{E_h}{\hbar}\right]\frac{1}{\alpha^2}\frac{\hbar}{c^2}\ ,$$

where $A_r(X) \equiv m(X)/m_u$, and we used the definition of the Hartree energy to rewrite the dependence on the electron mass. The relative uncertainties in $A_r(H)$, $A_r(e)$, and E_h are currently smaller than that of α.

In summary, we have described five experiments that determine four quantities. This is an overdetermined data set and checks for consistency. To date these checks are good to parts in 10^{10} and confirm the theory at this level. We stress, however, that the tests of fundamental theory are more wide ranging than suggested by the limited number of measurements. They include at least two implicit assumptions that are worth mentioning. The first is energy conservation and leads to the fact that the frequency of an emitted or absorbed photon equals the frequency difference of energy levels of the atom. A second assumption is that particles have a wave-like nature as well or, more precisely, that the momentum p of a massive particle or massless photon is inversely proportional to its reduced wavelength $\lambda\!\!\!^{-}$. In fact, $p = \hbar k$, where $k = 1/\lambda\!\!\!^{-}$ is the photon wavenumber. This relation combined with energy-momentum conservation underpins the atom recoil experiments.

29.3 Topics in This Review

The description of tests of QED in the previous section needs to be refined to include the role of small corrections and their parameters. For example, in hydrogen spectroscopy, the mass and charge radius of the proton must be considered. In g-factor measurements and hydrogen spectroscopy, virtual vacuum polarization loops containing the heavier muon and tau leptons, as well as quarks, lead to additional mass dependencies. The next sections summarize how these dependencies arise.

We only consider a subset of tests of QED. Some of the omitted topics are the spectroscopy of positronium, QED of highly-charged simple ions, Delbrück scattering of photons by nuclei, and helium fine structure. Positronium would suffer less from corrections due to hadronic effects. The theory, however, is more difficult due to the absence of a small parameter, such as the electron-to-proton mass ratio. Highly-charged ions are a means of studying strong field effects near their nucleus. Photon scattering by nuclei can create virtual lepton pairs in a domain beyond the Compton scattering process. The helium measurements are an independent means of determining the fine-structure constant. Some of these topics are covered in other chapters of this book. Although these topics may be considered equally important, our attention in this chapter is focused on the most precise tests of QED.

The remainder of this article has the following structure. Section 29.4 summarizes the required QED theory for the g-factor of the free electron and our ability to extract α. Section 29.5 then describes mass measurements by atom recoil experiments and mass-ratio measurements by atomic mass spectrometry for the heavier atoms. Mass-ratio determinations $m(Y)/m_e$ for light atoms are discussed in Sect. 29.6. The section also summarizes the theory of the electron g-factor in hydrogen-like ions. Combined, Sects. 29.5 and 29.6 lead to the most-accurate value for m_e. We finish with a discussion of QED theory for the hydrogen atom in Sect. 29.7.

29.4 Electron g-Factor Anomaly

The theoretical expression for the anomaly of the electron a_e(th) may be written as

$$a_e(\text{th}) = a_e(\text{QED}) + a_e(\text{weak}) + a_e(\text{had}) \,, \qquad (29.9)$$

where the terms denoted by "QED", "weak", and "had" account for the purely quantum electrodynamic, predominantly electroweak, and predominantly hadronic (that is, strong interaction) contributions to a_e, respectively. The QED contribution may be written as

$$a_e(\text{QED}) = \sum_{n=1}^{\infty} C_e^{(2n)} \left(\frac{\alpha}{\pi}\right)^n \,, \qquad (29.10)$$

where index n corresponds to contributions with n virtual photons. Here, $n > 5$ contributions can be neglected, and

$$C_e^{(2n)} = A_1^{(2n)} + A_2^{(2n)}(x_{e\mu}) + A_2^{(2n)}(x_{e\tau}) + \ldots \,, \qquad (29.11)$$

with coefficients $A_1^{(2n)}$ and functions $A_2^{(2n)}(x)$ evaluated at $x = x_{eX} \equiv m_e/m_X \ll 1$ for lepton $X = \mu$ or τ. For $n > 1$, the coefficients $A_1^{(2n)}$ include vacuum-polarization corrections with virtual electron/positron pairs, while $A_2^{(2n)}(x)$ are vacuum-polarization corrections due to heavier leptons. For $x \to 0$, we have $A_2^{(4)}(x) = x^2/45 + \mathcal{O}(x^4)$ and $A_2^{(6)}(x) = x^2(b_0 + b_1 \ln x) + \mathcal{O}(x^4)$ with $b_0 = 0.593274\ldots$ and $b_1 = 23/135$ [9, 10]. The $\mathcal{O}(x^4)$ contributions are known and included in the calculations but not reproduced here. The functions $A_2^{(8)}(x)$ and $A_2^{(10)}(x)$ are also $\mathcal{O}(x^2)$ for small x but are not reproduced here [11, 12]. Currently, vacuum-polarization corrections for the free-electron anomaly that depend on two lepton mass ratios can be neglected. Table 29.1 lists the relevant coefficients as used in the 2014 CODATA adjustment. Uncertainties in parenthesis here and elsewhere are combined one-standard-deviation statistical and systematic uncertainties. Additional references to the original literature can be found in the paper on the adjustment. It is worth noting that since 2014 the coefficient $A_1^{(8)}$ has been evaluated virtually exactly in a tremendous effort described in [13], while $A_2^{(10)}$ has been updated, shifting its value [14].

Table 29.1 Coefficients for the QED contributions to the electron anomaly. The coefficients $A_1^{(2n)}$ and functions $A_2^{(2n)}(x)$, evaluated at $x = x_{e\mu} \equiv m_e/m_\mu$ and $x_{e\tau} \equiv m_e/m_\tau$ for the muon and tau leptons, respectively, are listed with two significant digits for ease of comparison; summed values $C_e^{(2n)}$, based on the 2014 CODATA adjustment, are listed as accurately as needed for the tests described in this article. Missing values indicate that their contribution to the electron anomaly is negligible

n	$A_1^{(2n)}$	$A_2^{(2n)}(x_{e\mu})$	$A_2^{(2n)}(x_{e\tau})$	$C_e^{(2n)}$
1	1/2	0	0	0.5
2	−0.33	5.2×10^{-7}	1.8×10^{-9}	−0.32847844400...
3	1.2	-7.4×10^{-6}	-6.6×10^{-8}	1.181234017...
4	−1.9	9.2×10^{-4}	7.4×10^{-6}	−1.91206(84)
5	7.8	-3.8×10^{-3}		7.79(34)

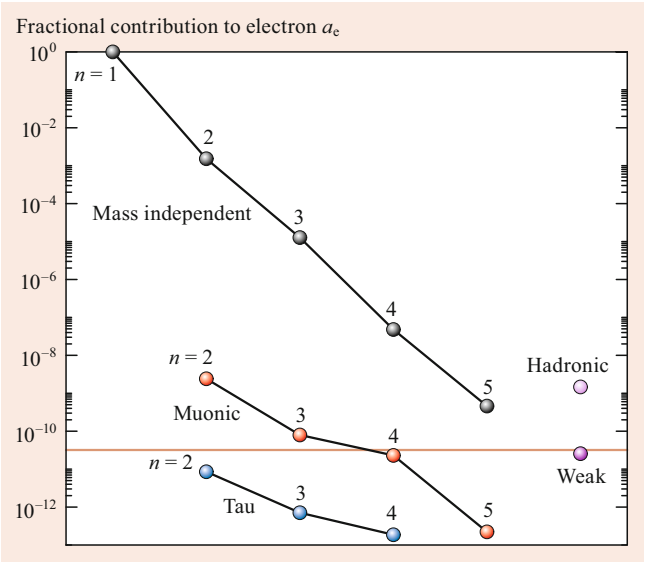

Fig. 29.4 Fractional absolute values of the contributions to the theoretical g-factor anomaly of the free electron. QED contributions are due to the mass-independent $A_1^{(2n)}$ (*black markers*), to the muon-dependent $A_2^{(2n)}(x_{e\mu})$ (*red markers*), and to the tau-dependent $A_2^{(2n)}(x_{e\tau})$ (*blue markers*) corrections, respectively. Contributions due to the weak and hadronic interactions are also shown. The *horizontal orange line* shows the relative uncertainty in the determination of a_e(th). The graph is based on the 2014 CODATA value for the fine-structure constant

The electroweak contribution is

$$a_e(\text{weak}) = 0.02973(23) \times 10^{-12} \qquad (29.12)$$

and is calculated as discussed in the 1998 CODATA adjustment but with the 2014 values of the Fermi coupling constant $G_F/(\hbar c)^3$ and the weak mixing angle θ_W [15]. The total hadronic contribution is

$$a_e(\text{had}) = 1.734(15) \times 10^{-12} \qquad (29.13)$$

and is a sum of multiple vacuum-polarization contributions.

Figure 29.4 shows a graphical representation of contributions to the electron anomaly. The QED corrections decrease roughly exponentially in size with order n for both mass-independent and dependent contributions. Contributions from virtual loops containing τ leptons are currently negligible. Weak and hadronic contributions are more important. The theoretical uncertainty of the anomaly (absent any uncertainty in the fine-structure constant) is dominated by two contributions: the mass-independent $n = 5$ QED correction and the hadronic contribution. In fact, it is given by

$$u[a_e(\text{th})] = 0.037 \times 10^{-12} = 0.32 \times 10^{-10}\, a_e \qquad (29.14)$$

and is significantly smaller than the uncertainty of the most-accurate experimental value of $2.4 \times 10^{-10} a_e$ [6]. Consequently, the relative uncertainty of the fine-structure constant is essentially the same as the experimental relative uncertainty. That is, equating the theoretical expression of $a_e(\text{th})$ and the experimental value yields

$$\alpha^{-1}(a_e) = 137.035999160(33) \quad [2.4 \times 10^{-10}] \,. \quad (29.15)$$

The number in square brackets is the relative uncertainty of the fine-structure constant, $u_r(\alpha) = u(\alpha)/\alpha$.

29.5 Atom Recoil Experiments and Mass Spectrometry

Atom recoil experiments are performed with the heavier alkali-metal atoms, ^{87}Rb and ^{133}Cs. These atoms have easily accessible atomic transitions in the optical frequency domain, with excited states that only decay back to the ground state and can, thus, be brought to a near standstill by laser cooling techniques. For the 2014 CODATA adjustment, the most accurate measurement relied on the ^{87}Rb isotope [16] and gave

$$\frac{m(^{87}\text{Rb})}{\hbar} = 1{,}368{,}480{,}428.9(1.7)\,\text{m}^{-2}\,\text{s} \quad [1.2 \times 10^{-9}] \,. \quad (29.16)$$

In the revised SI with a fixed reduced Planck constant, this translates into an equally accurate measurement of $m(^{87}\text{Rb})$ in kg. A 2018 value for $m(^{133}\text{Cs})/\hbar$ for atomic cesium with a three times smaller relative uncertainty is reported in [17].

In mass spectrometry, the most accurate measurements compare the mass of two or more low-charge-state ions. Over the years, these measurements have been performed for most stable and unstable atoms in the periodic table. After accounting for the mass of the electrons and binding energies, mass data for neutral atoms were collated in [18, 19] in the atomic mass unit m_u. For ^{87}Rb and ^{28}Si, this 2012 database gives

$$A_r(^{87}\text{Rb}) = \frac{m(^{87}\text{Rb})}{m_u} = 86.9091805319(65) \quad [7.5 \times 10^{-11}] \,, \quad (29.17)$$

and

$$A_r(^{28}\text{Si}) = 27.97692653465(44) \quad [1.6 \times 10^{-11}] \,, \quad (29.18)$$

respectively, which have a much smaller relative uncertainty than that for masses determined by atom recoil measurements. The improved 2016 evaluation can be found in [7, 20].

In any case, from this recoil measurement, we calculate

$$m(^{12}\text{C}) = m(^{87}\text{Rb}) \times \frac{12}{A_r(^{87}\text{Rb})} \quad (29.19)$$

in kg in the revised SI to determine $m(^{12}\text{C})$ with a relative uncertainty of 1.2×10^{-9} through error propagation. Similarly, relationships can be used for the mass of ^{28}Si.

29.6 Mass-Ratio Measurements Using the g-Factor of Hydrogen-Like Ions

Measurements of the spin-flip and cyclotron frequencies of ground-state hydrogen-like atomic ions in a homogeneous magnetic field are currently the most accurate means to determine atom-to-electron mass ratios. This method relies on the ability of theorists to calculate the g-factor of the bound electron accurately. This approach is competitive as long as the trapped ion is relatively light. Accounting for the electron removal energies of ions becomes prohibitively hard for heavy atoms. Similarly, computing the g-factor within the framework of relativistic QED bound-state theory is more complex for heavier hydrogen-like ions as corrections with higher powers in $Z\alpha$ are more important. For nuclei with zero nuclear spin, the mass ratio follows from rearranging Eq. (29.8) to

$$\frac{m(Y^{q+})}{m_e} = -2q \frac{1}{g_Y(\alpha, \ldots)} \frac{\omega_s(Y^{q+})}{\omega_c(Y^{q+})}\bigg|_{\text{exp}} \quad (29.20)$$

and

$$\frac{m(Y)}{m_e} = \frac{m(Y^{q+})}{m_e} + q - \sum_{m=0}^{q-1} \frac{E_I(Y^{m+})}{m_e c^2} \,, \quad (29.21)$$

where $E_I(Y^{m+})$ is the positive ionization energy of ion Y^{m+}, and we recall that $q = Z_Y - 1$.

A broad program involving researchers from a number of European laboratories has measured spin-flip and cyclotron frequency ratios and calculated the g-factor for different ions, most notably $^{12}\text{C}^{5+}$ and $^{28}\text{Si}^{13+}$. The measurements themselves were performed at the Max-Planck Institut für Kernphysik (MPIK), Heidelberg, Germany. Recently reported values are [21, 22]

$$\frac{\omega_s(^{12}\text{C}^{5+})}{\omega_c(^{12}\text{C}^{5+})} = 4376.21050087(12) \quad [2.8 \times 10^{-11}] \,, \quad (29.22)$$

and [23]

$$\frac{\omega_s(^{28}\text{Si}^{13+})}{\omega_c(^{28}\text{Si}^{13+})} = 3912.86606484(19) \quad [4.8 \times 10^{-11}] \,. \quad (29.23)$$

These two frequency ratios are correlated with a correlation coefficient $r = 0.347$ mainly due to image charge corrections [24]. The authors of [24] also slightly reassessed the values given in the original references. The reassessed values are quoted here.

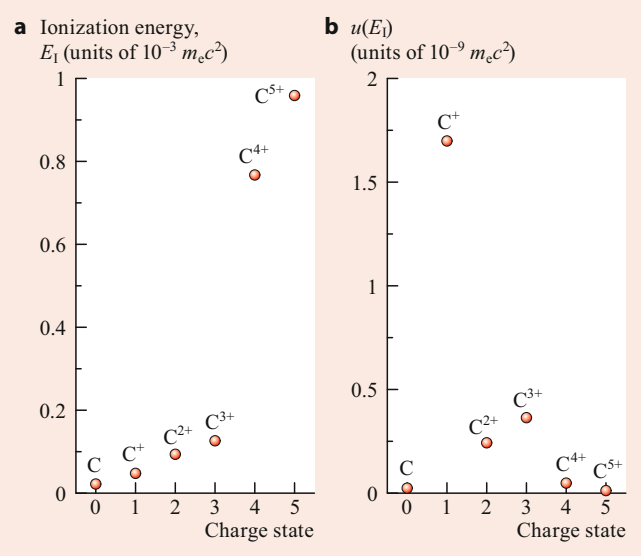

Fig. 29.5 Ionization energies (**a**) and their uncertainties (**b**) of the six charge states $^{12}C^{m+}$ of carbon-12 expressed in units of $m_e c^2$. Notice the large difference in scale between the two panels. In practice, ionization energies, E_I, are reported in units of hc. The unit conversion of the energies and their uncertainties is based on the identity $E/(m_e c^2) = \alpha^2/(2R_\infty) \times E/(hc)$, where R_∞ is the Rydberg constant, and we observe that $\alpha^2/(2R_\infty)$, with a relative uncertainty of 5×10^{-10}, does not increase the uncertainty of the E_I

The theoretical electron g-factors for $^{12}C^{5+}$ and $^{28}Si^{13+}$ have a relative uncertainty of 1.3×10^{-11} and 8.5×10^{-10}, respectively, as explained in the next section. Hence, the relative uncertainty for the mass ratio m_{Yq+}/m_e is 3.0×10^{-11} and 8.5×10^{-10} for these two ions, respectively. Next, we use Eq. (29.21) to determine the neutral atom to electron mass ratio. Figure 29.5 shows the ionization energies and their uncertainties for all charge states of ^{12}C in units of $m_e c^2$. We observe that, as expected, the ionization energy increases with charge state, but that, possibly surprisingly, the ionization energy with the largest uncertainty by far is that for the singly charged carbon ion. The ionization energies are added to give the electron removal energy $\Delta E_B = 1.0569819(18) \times 10^{-3} m_e c^2$ from ^{12}C to $^{12}C^{5+}$.

We combine the results of Sects. 29.5 and 29.6 to find the values

$$\frac{m(^{12}C)}{m_e} = 21{,}874.66183428(66) \quad [3.0 \times 10^{-11}]$$

and

$$\frac{m_e}{\hbar} = \frac{m_e}{m(^{12}C)} \frac{m(^{12}C)}{m(^{87}Rb)} \frac{m(^{87}Rb)}{\hbar} = 8.637992726(11) \times 10^3\ \mathrm{m^{-2}\,s} \quad [1.2 \times 10^{-9}]\,. \tag{29.24}$$

We observe that the removal energy ΔE_B has a measurable effect on the mass of the carbon-12 atom but that the uncertainty of $m_e/\hbar$ is currently limited by the atom recoil experiment. An evaluation of $m_e/\hbar$ based on ^{28}Si data gives a consistent value with only a slightly larger uncertainty. The two values can be combined to find more accurate values for $m(^{12}C)/m_e$ and $m_e/\hbar$ as long as the strong correlations between the uncertainties of the g-factor, as well as those of the frequency ratio ω_s/ω_c, are taken into account. With the 2018 atom recoil experiments with ^{133}Cs [17], the uncertainty of $m_e/\hbar$ has improved by a factor of 3.

29.6.1 Theory for the g-Factor of Hydrogen-Like Ions

We summarize the contributions to the theoretical description of the electron g-factor of ground S-state hydrogen-like ions. The main contributions to the g-factor can be categorized as

$$g_Y = g_D + \Delta g_{rad} + \Delta g_{rec} + \Delta g_{ns} + \dots\,, \tag{29.25}$$

where g_D is the Dirac (relativistic) value, and Δg_{rad}, Δg_{rec}, and Δg_{ns} are due to radiative, recoil, and nuclear size corrections, respectively. Other corrections, indicated by the dots, are negligible at this time. Numerical results for the various contributions are summarized in Table 29.2 for $^{12}C^{5+}$ and Table 29.3 for $^{28}Si^{13+}$.

The Dirac value is known exactly [25] from the Dirac equation for an electron in the field of a fixed point charge of magnitude Ze, where, for clarity, we omit subscript Y on Z for the remainder of this section. Its value is

$$g_D = -\frac{2}{3}\left[1 + 2\sqrt{1 - (Z\alpha)^2}\right], \tag{29.26}$$

with an uncertainty that is solely due to the uncertainty in α. Radiative corrections may be written as

$$\Delta g_{rad} = -2 \sum_{n=1} C_e^{(2n)}(Z\alpha) \left(\frac{\alpha}{\pi}\right)^n, \tag{29.27}$$

where the functions $C_e^{(2n)}(x)$ are evaluated at $x = Z\alpha$, correspond to contributions with n virtual photons, and are slowly varying functions of x. They are related to the coefficients for the free electron $C_e^{(2n)}$, defined in Sect. 29.4, by

$$\lim_{x \to 0} C_e^{(2n)}(x) = C_e^{(2n)}\,. \tag{29.28}$$

The function $C_e^{(2)}(x)$ is computed as the sum of three contributions. The first contribution is a self-energy correction given by

$$C_{e,SE}^{(2)}(x) = \frac{1}{2}\left\{1 + \frac{1}{6}x^2 + x^4\left[\frac{32}{9}\ln(x^{-2}) + \frac{247}{216} - \frac{8}{9}\ln k_0 - \frac{8}{3}\ln k_3\right] + x^5 R_{SE}(x)\right\}, \tag{29.29}$$

where $\ln k_0 = 2.984128556$ and $\ln k_3 = 3.272806545$. Values for the remainder function $R_{\rm SE}(x)$ are based on extrapolations from numerical calculations at high Z. In particular, $R_{\rm SE}(6\alpha) = 22.160(10)$ and $R_{\rm SE}(14\alpha) = 20.999(2)$ based on the 2014 CODATA adjustment. In 2017, the values for $R_{\rm SE}(x)$ were significantly improved [26].

The second and third contributions to $C_{\rm e}^{(2)}(x)$ are two lowest-order vacuum-polarization corrections [27]. In the second "wave function" correction, the vacuum polarization loop modifies the interaction between the bound electron and the Coulomb field of the nucleus, and in the third "potential" correction, the loop modifies the interaction between the bound electron and the external magnetic field. The sum of the one-photon vacuum polarization contributions are

$$C_{\rm e,VP}^{(2)}(6\alpha) = -0.000001832142(12)\,, \tag{29.30}$$

and

$$C_{\rm e,VP}^{(2)}(14\alpha) = -0.0000505452(11)\,, \tag{29.31}$$

for $^{12}C^{5+}$ and $^{28}Si^{13+}$, respectively.

The $n = 2$ two-photon correction for the ground S-state is [28, 29]

$$\begin{aligned} C_{\rm e}^{(4)}(x) &= \left(1 + \frac{x^2}{6}\right) C_{\rm e}^{(4)} \\ &\quad + x^4 \left[\frac{14}{9}\,\ln(x^{-2}) + \frac{991{,}343}{155{,}520} - \frac{2}{9}\,\ln k_0 - \frac{4}{3}\,\ln k_3 \right. \\ &\quad \left. + \frac{679\,\pi^2}{12{,}960} - \frac{1441\,\pi^2}{720}\,\ln 2 + \frac{1441}{480}\,\zeta(3)\right] + \mathcal{O}(x^5) \\ &= \begin{cases} -0.3285778(23) & \text{for } x = 6\alpha \\ -0.32917(15) & \text{for } x = 14\alpha \end{cases}, \end{aligned} \tag{29.32}$$

where $\zeta(z)$ is the Riemann zeta function. The quoted uncertainty is an estimate of uncalculated higher-order contributions given by [28]

$$u\left[C_{\rm e}^{(4)}(x)\right] = 2\left|x^5\, C_{\rm e}^{(4)}\, R_{\rm SE}(x)\right|\,. \tag{29.33}$$

Since the remainder function differs only by about one percent for carbon and silicon, the main Z (or x) dependence of the uncertainty is given by x^5, and we assume that the uncertainty of the two-photon correction is completely correlated for the two ions. The authors of [30, 31] calculated some of the two-loop vacuum polarization diagrams of order x^5 and found them to be on the order of the uncertainty in Eq. (29.32). The authors of [32] computed an additional light-by-light contribution to $C_{\rm e}^{(4)}(x)$, which shifts its value within its uncertainty. It is not included here.

The leading binding correction to $C_{\rm e}^{(2n)}(x)$ is

$$C_{\rm e}^{(2n)}(x) = \left(1 + \frac{x^2}{6} + \ldots\right) C_{\rm e}^{(2n)}\,, \tag{29.34}$$

for *any* n. This surprising result was derived in [33, 34], and for $n = 1$ and 2 it is evident from Eqs. (29.29) and (29.32). As the uncertainty due to uncalculated higher-order terms is negligible we use $C_{\rm e}^{(2n)}(x) \to (1 + x^2/6) C_{\rm e}^{(2n)}$ for the three, four, and five ($n = 3$, 4, and 5) photon contributions with an uncertainty solely determined by the uncertainty of $C_{\rm e}^{(2n)}$ in Table 29.1.

The corrections $g_{\rm D}$ and $\Delta g_{\rm rad}$ are based on the assumption that nuclei have an infinite mass. The recoil correction to the g-factor associated with a finite mass is

$$\Delta g_{\rm rec} = \Delta g_{\rm rec}^{(0)} + \Delta g_{\rm rec}^{(2)}\,, \tag{29.35}$$

corresponding to terms that are zero-order and first-order in α/π, respectively. For $\Delta g_{\rm rec}^{(0)}$, we have

$$\begin{aligned} \Delta g_{\rm rec}^{(0)} &= \left\{-(Z\alpha)^2 + \frac{(Z\alpha)^4}{3[1+\sqrt{1-(Z\alpha)^2}]^2} - (Z\alpha)^5\, P(Z\alpha)\right\} \\ &\quad \times \frac{m_{\rm e}}{m_{\rm N}} + (1+Z)(Z\alpha)^2 \left(\frac{m_{\rm e}}{m_{\rm N}}\right)^2\,, \end{aligned} \tag{29.36}$$

where $m_{\rm N}$ is the mass of the nucleus. Mass ratios, based on the 2014 adjustment values of the constants, are $m_{\rm e}/m(^{12}C^{6+}) = 0.0000457275\ldots$ and $m_{\rm e}/m(^{28}Si^{14+}) = 0.0000196136\ldots$ The authors of [35] evaluated the function $P(x)$ numerically for a discrete set of $x < 1$, with the result $P(6\alpha) = 10.49395(1)$ for hydrogenic carbon. For silicon, we use the interpolated value $P(14\alpha) = 7.16223(1)$. For $\Delta g_{\rm rec}^{(2)}$, we have

$$\Delta g_{\rm rec}^{(2)} = \frac{\alpha}{\pi}\,\frac{(Z\alpha)^2}{3}\,\frac{m_{\rm e}}{m_{\rm N}}\,. \tag{29.37}$$

The uncertainty in $\Delta g_{\rm rec}^{(2)}$ is negligible compared to that of $\Delta g_{\rm rad}^{(2)}$.

Finally, the finite size of the nucleus leads to a small correction to the g-factor given by [36]

$$\Delta g_{\rm ns} = -\frac{8}{3}(Z\alpha)^4 \left(\frac{r_{\rm N}}{\lambda\!\!\!^{-}_{\rm C}}\right)^2 + \ldots\,, \tag{29.38}$$

where $r_{\rm N}$ is the nuclear rms charge radius, and $\lambda\!\!\!^{-}_{\rm C} = \hbar/(m_{\rm e}c)$ is the reduced Compton wavelength of the electron. The authors of [37] calculated additional corrections but gave numerical values for $\Delta g_{\rm ns}$ based on early $r_{\rm N}$ values. We incorporate their corrections using an $(r_{\rm N})^2$ scaling and the updated $r_{\rm N} = 2.4703(22)$ fm and $r_{\rm N} = 3.1223(24)$ fm for ^{12}C and ^{28}Si, respectively [38].

The theoretical value for the g-factor of the electron in hydrogen-like carbon 12 or silicon 28 is the sum of the individual contributions discussed above and summarized in Tables 29.2 and 29.3. For each contribution the tables also list the uncertainty. For both ions the uncertainty is dominated by

Table 29.2 Theoretical contributions and total value for the g-factor of hydrogenic carbon 12 based on the 2014 CODATA recommended values of the constants and corresponding theory. The total g-factor has a relative uncertainty of 1.3×10^{-11}

Contribution	Value	Source
Dirac g_D	−1.99872135439 21(6)	Eq. (29.26)
$\Delta g_{SE}^{(2)}$	−0.002323672435(4)	Eq. (29.29)
$\Delta g_{VP}^{(2)}$	0.000000008511	Eq. (29.30)
$\Delta g^{(4)}$	0.000003545677(25)	Eq. (29.32)
$\Delta g^{(6)}$	−0.000000029618	Eq. (29.34)
$\Delta g^{(8)}$	0.000000000111	Eq. (29.34)
$\Delta g^{(10)}$	−0.000000000001	Eq. (29.34)
Δg_{rec}	−0.000000087629	Eq. (29.35)
Δg_{ns}	−0.000000000408(1)	Eq. (29.38)
$g(^{12}C^{5+})$	−2.001041590183(26)	

Table 29.3 Theoretical contributions and total value for the g-factor of hydrogenic silicon 28 based on the 2014 CODATA recommended values of the constants and corresponding theory. The total g-factor has a relative uncertainty of 8.5×10^{-10}

Contribution	Value	Source
Dirac g_D	−1.993023571557(3)	Eq. (29.26)
$\Delta g_{SE}^{(2)}$	−0.00232891747(5)	Eq. (29.29)
$\Delta g_{VP}^{(2)}$	0.00000023481(1)	Eq. (29.31)
$\Delta g^{(4)}$	0.0000035521(17)	Eq. (29.32)
$\Delta g^{(6)}$	−0.00000002966	Eq. (29.34)
$\Delta g^{(8)}$	0.00000000011	Eq. (29.34)
$\Delta g^{(10)}$	−0.00000000000	Eq. (29.34)
Δg_{rec}	−0.00000020588	Eq. (29.35)
Δg_{ns}	−0.00000002053(3)	Eq. (29.38)
$g(^{28}Si^{13+})$	−1.9953489581(17)	

that of the two-photon $n = 2$ correction $\Delta g^{(4)}$. The relative uncertainties of the $^{12}C^{5+}$ and $^{28}Si^{13+}$ values are 1.3×10^{-11} and 8.5×10^{-10}, respectively, sufficient for the purpose of determining competitive atom-to-electron mass ratios. Finally, the two g-factors have a correlation coefficient $r = 0.79$.

29.7 Hydrogen Atom Energy levels

Measurements of the hydrogen energy levels are currently the most precise way to determine the Hartree energy divided by the reduced Planck constant or, equivalently, the Rydberg constant. The measurements also help determine α and the proton charge radius. The eigenstates are labeled by $n\ell_j$, where $n = 1, 2, \ldots$ is the principal quantum number, $\ell = 0, 1, \ldots, n-1$ is the nonrelativistic angular momentum quantum number, and j is the total angular momentum quantum number. Their energies are denoted by $E(n\ell_j)$ and, following the usual convention, we use S, P, D, ... to denote $\ell = 0, 1, 2, \ldots$ states. Our discussion will omit hyperfine effects from coupling of the electron to the magnetic and other moments of the proton, as at 2014 accuracy levels they can easily be accounted for.

The world's best-known optical transition frequency is that for the $1S_{1/2}$–$2S_{1/2}$ Lyman-alpha line of hydrogen, which has been obtained by an experimental group in Garching, Germany [39, 40]. They quote

$$\omega_H(1S_{1/2}\text{–}2S_{1/2}) = 2\pi \times 2{,}466{,}061{,}413{,}187{,}035(10)\,\text{rad/s} \quad [4.2 \times 10^{-15}]$$

or

$$\nu_H(1S_{1/2}\text{–}2S_{1/2}) = 2{,}466{,}061{,}413{,}187{,}035(10)\,\text{Hz}$$

in 2011 and

$$\omega_H(1S_{1/2}\text{–}2S_{1/2}) = 2\pi \times 2{,}466{,}061{,}413{,}187{,}018(11)\,\text{rad/s} \quad [4.4 \times 10^{-15}]$$

or

$$\nu_H(1S_{1/2}\text{–}2S_{1/2}) = 2{,}466{,}061{,}413{,}187{,}018(11)\,\text{Hz}$$

in 2013. The two values are correlated with a correlation coefficient $r = 0.707$ [41].

The frequency of this Lyman-alpha line is known to almost 15 significant digits. The analytical, theoretical determination of this transition frequency, which in its simplest description by Bohr equals $3E_h/(8h)$, is equally impressive, although less accurate. It has 13 contributions ranging from the Dirac eigenvalue, QED corrections with one or more virtual photons and lepton-antilepton pairs, as well as nuclear size and recoil effects. Figure 29.6a gives a visual representation of the size and uncertainties of these contributions. We postpone the discussion of the name for and mathematical form of each of the corrections until Sect. 29.7.1. The sizes of the contributions vary by orders of magnitude, although size is not necessarily an indication of its uncertainty. The uncertainty of both the Dirac energy and the correction due to the proton charge radius are the largest at ≈ 10 kHz and reflect the uncertainty of constants $E_h/\hbar$ and r_p, respectively. The largest theoretical uncertainties are in the two-photon and three-photon corrections and reflect uncomputed terms. (The individual uncertainties of the Dirac energy and correction due to the proton charge radius are large compared to that of the experimental $1S_{1/2}$–$2S_{1/2}$ transition frequency. As a result the uncertainties are highly correlated with a correlation coefficient very close to one.)

The $2P_{1/2}$–$2S_{1/2}$ transition, or Lamb shift, is equally important, because the Dirac or Bohr energies cancel, and the dominant contribution by far is the self-energy correction, a QED correction where the bound electron emits and absorbs a virtual photon. It is of order $\alpha^3 E_h$ as seen in Sect. 29.7.1. The energy contributions to this transition are shown in Fig. 29.6b, while the two best measurements of this transition frequency are

$$\nu_H(2P_{1/2}\text{–}2S_{1/2}) = 1{,}057{,}845.0(9.0)\,\text{kHz} \quad [8.5 \times 10^{-6}]$$

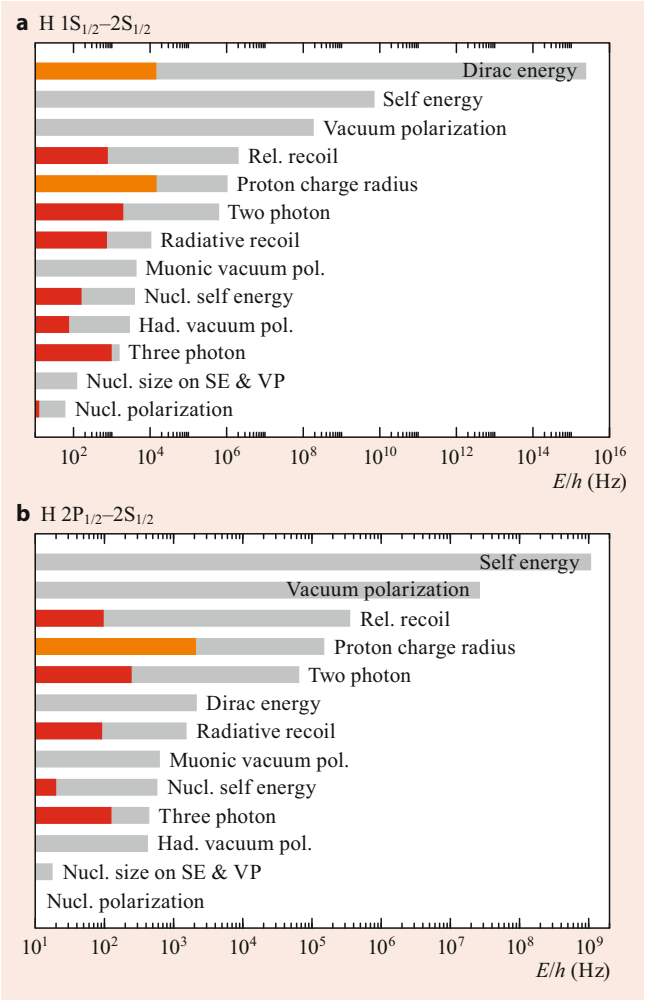

Fig. 29.6 Absolute value of the 13 contributions (*gray bars*) and their uncertainty (*red* and *orange bars*) to the hydrogen $1S_{1/2}$–$2S_{1/2}$ (**a**) and $2P_{1/2}$–$2S_{1/2}$ (**b**) transition frequencies on a logarithmic scale. The values are sorted by the size of the contribution. The label next to each contribution is defined in the text. The uncertainty of a contribution is either fully due to the uncertainty of constants within QED theory, here the Hartree frequency, $E_h/\hbar$, and proton charge radius (*orange bars*), or by the estimated value of missing or uncomputed terms (*red bars*). The two transition frequencies have been measured to 10 and 9 kHz, respectively

and

$$\nu_H(2P_{1/2}\text{–}2S_{1/2}) = 1{,}057{,}862(20)\,\text{kHz} \quad [1.9\times10^{-5}]\,,$$

from research groups at Harvard University [42] and the University of Sussex [43], respectively. The theoretical value for this transition from the 2014 CODATA least-squares adjustment is

$$\nu_H(2P_{1/2}\text{–}2S_{1/2}) = 1{,}057{,}843.7(2.1)\,\text{kHz} \quad [2.0\times10^{-6}]$$

and is in agreement with the experiments. The largest contribution to the theoretical uncertainty is due to the uncertainty in the proton charge radius, while uncertainties from uncomputed terms in the two-photon and three-photon corrections are much smaller than the experimental uncertainty.

In a naive least-squares adjustment that includes only these two transitions, the Lyman-alpha line and Lamb shift determine (relatively inaccurate) values for α and m_e. Data on other transitions and the measurements discussed in the previous sections significantly decrease their uncertainties, constrain the value for the proton charge radius, and check for consistency. Indeed, the focus has shifted to complementary transitions in H [44, 45] and measurements on and theory of muonic-hydrogen with the goal of resolving the discrepancies in the determination of the charge radius of the proton. In the 2014, CODATA adjustment muonic-hydrogen data was not included.

29.7.1 Theory for the Hydrogen Energy Levels

Theoretical values for hydrogen energy levels as for the bound-electron g-factor are determined by the Dirac eigenvalue, QED effects such as self-energy and vacuum polarization, and proton size and motion or recoil effects. Theoretical energies of different states are correlated. For example, for S-states, uncalculated contributions are primarily of the form of an unknown constant divided by n^3. This is taken into account by using covariances between levels in addition to the uncertainties of the individual levels. Hence, we distinguish between components of uncertainty that are proportional to $1/n^3$ and those that are uncorrelated, where necessary. They are denoted by u_0 and u_n, respectively.

We now consider each of the contributions to the energy in turn, as well as explain how to combine the uncertainties of the contributions. Table 29.4 gives a list of the contributions, their size both in terms of fundamental constants, as well as order-of-magnitude numerical values for the $1S_{1/2}$–$2S_{1/2}$ transition.

Dirac Eigenvalue

The energy of an electron in a static Coulomb field with charge Ze with infinite mass is predominantly determined by the relativistic Dirac eigenvalue

$$E_D = f(n,\kappa)m_e c^2\,, \tag{29.39}$$

where

$$f(n,\kappa) = \left[1+\frac{(Z\alpha)^2}{(n-\delta)^2}\right]^{-1/2}\,, \tag{29.40}$$

with defect $\delta = |\kappa| - \sqrt{\kappa^2-(Z\alpha)^2}$ and κ is the angular momentum-parity quantum number ($\kappa = -1, 1, -2, 2, -3$ for $S_{1/2}$, $P_{1/2}$, $P_{3/2}$, $D_{3/2}$, and $D_{5/2}$-states, respectively). States

Table 29.4 List of contributions and their main dependence on fundamental constants to the hydrogen transition frequencies ordered by appearance in the text. The first two columns give the section in Sec. 29.7.1 in which the contribution is described in detail and the name of the contribution, respectively. The fundamental-constant dependence of a contribution in the third column is given in terms of the Hartree energy $E_h = m_e c^2 \alpha^2$ and four dimensionless variables with values small compared to one: the fine-structure constant α, the proton charge radius divided by the reduced Compton wavelength $r_p/\lambda\!\!\!^{-}_C$, and the mass ratios m_e/m_μ and m_e/m_p. The last column gives the order of magnitude of each of the contributions in Hz for the $1S_{1/2}$–$2S_{1/2}$ transition

	Contribution	Scaling	Δ/h (Hz)
a	Dirac energy	E_h	10^{15}
b	Relativistic recoil	$(m_e/m_p)\alpha^3\ E_h$	10^6
c	Nuclear polarizability	–	10^2
d	Self-energy	$\alpha^3\ E_h$	10^{10}
e	Vacuum polarization	$\alpha^3\ E_h$	10^8
e	Muon vacuum polarization	$(m_e/m_\mu)^2\alpha^3\ E_h$	10^4
e	Hadronic vacuum pol.	–	10^3
f	Two-photon	$\alpha^4\ E_h$	10^6
g	Three-photon	$\alpha^5\ E_h$	10^3
h	Nuclear size	$(r_p/\lambda\!\!\!^{-}_C)^2\alpha^2\ E_h$	10^6
i	Nucl. size on SE & VP	$(r_p/\lambda\!\!\!^{-}_C)^2\alpha^4\ E_h$	10^2
j	Radiative recoil	$(m_e/m_p)\alpha^4\ E_h$	10^4
k	Nuclear self-energy	$(m_e/m_p)^2\alpha^3\ E_h$	10^3

with the same n and $j = |\kappa| - 1/2$ have degenerate eigenvalues. Finally, $\ell = |\kappa + 1/2| - 1/2$, and we retain the atomic number Z in the equations in order to classify the various contributions to the energies.

Corrections to the Dirac eigenvalue that approximately take into account the finite mass of the proton m_p are included in a more general expression for atomic energy levels. That is, we replace Eq. (29.39) by [46, 47]

$$E_M = Mc^2 + \left\{ f(n,\kappa) - 1 - \frac{1}{2}[f(n,\kappa)-1]^2 \frac{m_r}{M} + \frac{1}{2}\frac{1-\delta_{\ell 0}}{\kappa(2\ell+1)}\frac{(Z\alpha)^4}{n^3}\frac{m_r^2}{m_p^2} + \ldots \right\} m_r c^2 \,, \tag{29.41}$$

where $M = m_e + m_p$ and $m_r = m_e m_p/(m_e + m_p)$ is the reduced mass. Note that in this equation, the energy of $nS_{1/2}$-states differs from that of $nP_{1/2}$-states.

Relativistic Recoil

The leading relativistic-recoil correction, to lowest order in $Z\alpha$ and all orders in m_e/m_p, is [47, 48]

$$E_S = \frac{m_r^3}{m_e^2 m_p}\frac{(Z\alpha)^5}{\pi n^3} m_e c^2 \times \left\{ \frac{1}{3}\delta_{\ell 0}\ln(Z\alpha)^{-2} - \frac{8}{3}\ln k_0(n,\ell) - \frac{1}{9}\delta_{\ell 0} - \frac{7}{3}a_n - \frac{2}{m_p^2 - m_e^2}\delta_{\ell 0}\left[m_p^2 \ln\left(\frac{m_e}{m_r}\right) - m_e^2 \ln\left(\frac{m_p}{m_r}\right)\right]\right\} , \tag{29.42}$$

Table 29.5 Values of the Bethe logarithms $\ln k_0(n,\ell)$. Missing entries correspond to states for which no experimental measurements are available

n	S	P	D
1	2.984128556		
2	2.811769893	−0.030016709	
3	2.767663612		
4	2.749811840	−0.041954895	−0.006740939
6	2.735664207		−0.008147204
8	2.730267261		−0.008785043
12			−0.009342954

where $a_n = -2\ln(2/n) - 2 + 1/n - 2\sum_{i=1}^{n}(1/i)$ for $\ell = 0$ and $a_n = 1/[\ell(\ell+1)(2\ell+1)]$ otherwise. Values for the Bethe logarithms $\ln k_0(n,\ell)$ are given in Table 29.5.

Additional contributions to lowest order in the mass ratio and of higher order in $Z\alpha$ are

$$E_R = \frac{m_e}{m_p}\frac{(Z\alpha)^6}{n^3} m_e c^2 \left[D_{60} + D_{72} Z\alpha \ln^2 (Z\alpha)^{-2} + \ldots \right] , \tag{29.43}$$

where $D_{60} = 4\ln 2 - 7/2$ for $\ell = 0$ and $D_{60} = 2\left[3 - \ell(\ell+1)/n^2\right]/[(2\ell-1)(2\ell+1)(2\ell+3)]$ otherwise. Finally, $D_{72} = -11/(60\pi)\,\delta_{\ell 0}$. Recently, the coefficients D_{71} and D_{70} have been computed [49, 50], where, in particular, the D_{71} was found to be surprisingly large. In [49], the nuclear-size correction to $E_S + E_R$ was also computed.

The uncertainty in the relativistic recoil correction $E_S + E_R$ is

$$[0.1\delta_{\ell 0} + 0.01(1 - \delta_{\ell 0})]E_R \,. \tag{29.44}$$

Covariances follow from the $1/n^3$ scaling of the uncertainty.

Nuclear Polarizability

For the energy correction due to the nuclear polarizability in hydrogen, we use

$$E_P(\mathrm{H}) = -0.070(13)h\,\frac{\delta_{\ell 0}}{n^3}\,\mathrm{kHz} \,. \tag{29.45}$$

The effect is neglected for states of higher ℓ.

Self-Energy

The one-photon self-energy of an electron bound to a stationary point nucleus is

$$E_{SE}^{(2)} = \frac{\alpha}{\pi}\frac{(Z\alpha)^4}{n^3} F(Z\alpha)\, m_e c^2 \,, \tag{29.46}$$

where the function

$$F(x) = A_{41}\ln(x^{-2}) + A_{40} + A_{50}\,x + A_{62}\,x^2\ln^2(x^{-2}) + A_{61}\,x^2\ln(x^{-2}) + G_{SE}(x)\,x^2 \,, \tag{29.47}$$

with $A_{41} = 4/3\,\delta_{\ell 0}$, and $A_{40} = -(4/3)\ln k_0(n,\ell) + 10/9$ for $\ell = 0$ and $-(4/3)\ln k_0(n,\ell) - 1/[2\kappa(2\ell+1)]$ otherwise. Next, $A_{50} = (139/32 - 2\ln 2)\pi\,\delta_{\ell 0}$, $A_{62} = -\delta_{\ell 0}$, and

$$A_{61} = \left[4\left(1 + \frac{1}{2} + \cdots + \frac{1}{n}\right) + \frac{28}{3}\ln 2 - 4\ln n - \frac{601}{180} - \frac{77}{45n^2}\right]\delta_{\ell 0} + \frac{n^2-1}{n^2}\left(\frac{2}{15} + \frac{1}{3}\,\delta_{j\frac{1}{2}}\right)\delta_{\ell 1} + \frac{\left[96n^2 - 32\ell(\ell+1)\right](1-\delta_{\ell 0})}{3n^2(2\ell-1)(2\ell)(2\ell+1)(2\ell+2)(2\ell+3)} .$$

Values for $G_{\rm SE}(\alpha)$ in Eq. (29.47) are listed in Table 29.6. The uncertainty of the self-energy contribution is due to the uncertainty of $G_{\rm SE}(\alpha)$ listed in the table and is taken to be type u_n. See [51] for details.

Following convention, $F(Z\alpha)$ is multiplied by the factor $(m_{\rm r}/m_{\rm e})^3$, except the magnetic moment term $-1/[2\kappa(2\ell+1)]$ in A_{40}, which is instead multiplied by the factor $(m_{\rm r}/m_{\rm e})^2$, and the argument $(Z\alpha)^{-2}$ of the logarithms is replaced by $(m_{\rm e}/m_{\rm r})(Z\alpha)^{-2}$.

Vacuum Polarization

The stationary point nucleus second-order vacuum-polarization level shift is

$$E^{(2)}_{\rm VP} = \frac{\alpha}{\pi}\frac{(Z\alpha)^4}{n^3}H(Z\alpha)\,m_{\rm e}c^2 , \qquad (29.48)$$

where $H(x) = H^{(1)}(x) + H^{(\rm R)}(x)$ with

$$H^{(1)}(x) = V_{40} + V_{50}\,x + V_{61}\,x^2\ln(x^{-2}) + G^{(1)}_{\rm VP}(x)\,x^2 ,$$

with $V_{40} = -4/15\,\delta_{\ell 0}$, $V_{50} = 5\pi/48\,\delta_{\ell 0}$, and $V_{61} = -2/15\,\delta_{\ell 0}$. Values of $G^{(1)}_{\rm VP}(\alpha)$ are given in Table 29.7. Moreover, $H^{(\rm R)}(x) = G^{(\rm R)}_{\rm VP}(x)\,x^2$ with

$$G^{(\rm R)}_{\rm VP}(x) = \frac{19}{45} - \frac{\pi^2}{27} + \left(\frac{1}{16} - \frac{31\pi^2}{2880}\right)\pi\,x + \ldots , \qquad (29.49)$$

for $\ell = 0$ and zero otherwise. Higher-order terms are negligible. We multiply Eq. (29.48) by $(m_{\rm r}/m_{\rm e})^3$ and include a factor of $(m_{\rm e}/m_{\rm r})$ in the argument of the logarithm of the term proportional to V_{61}.

Vacuum polarization from $\mu^+\mu^-$ pairs is

$$E^{(2)}_{\mu\rm VP} = \frac{\alpha}{\pi}\frac{(Z\alpha)^4}{n^3}\left[-\frac{4}{15}\,\delta_{\ell 0}\right]\left(\frac{m_{\rm e}}{m_\mu}\right)^2\left(\frac{m_{\rm r}}{m_{\rm e}}\right)^3 m_{\rm e}c^2 + \ldots , \qquad (29.50)$$

while the hadronic vacuum polarization is given by

$$E^{(2)}_{\rm had\,VP} = 0.671(15)\,E^{(2)}_{\mu\rm VP} . \qquad (29.51)$$

Uncertainties are of type u_0. The muonic and hadronic vacuum-polarization contributions are negligible for higher-ℓ-states.

Two-Photon Corrections

The two-photon correction is

$$E^{(4)} = \left(\frac{\alpha}{\pi}\right)^2\frac{(Z\alpha)^4}{n^3}m_{\rm e}c^2F^{(4)}(Z\alpha) , \qquad (29.52)$$

where

$$F^{(4)}(x) = B_{40} + B_{50}\,x + B_{63}\,x^2\ln^3(x^{-2}) + B_{62}\,x^2\ln^2(x^{-2}) + B_{61}\,x^2\ln(x^{-2}) + B_{60}\,x^2 + B_{72}\,x^3\ln^2(x^{-2}) + B_{71}\,x^3\ln(x^{-2}) + \ldots ,$$

with

$$B_{40} = \left[\frac{3\pi^2}{2}\ln 2 - \frac{10\pi^2}{27} - \frac{2179}{648} - \frac{9}{4}\zeta(3)\right]\delta_{\ell 0} + \left[\frac{\pi^2\ln 2}{2} - \frac{\pi^2}{12} - \frac{197}{144} - \frac{3\zeta(3)}{4}\right]\frac{1-\delta_{\ell 0}}{\kappa(2\ell+1)} ,$$

$B_{50} = -21.55447(13)\,\delta_{\ell 0}$, $B_{63} = -8/27\,\delta_{\ell 0}$, and

$$B_{62} = \frac{16}{9}\left[\frac{71}{60} - \ln 2 + \psi(n) + \gamma - \ln n - \frac{1}{n} + \frac{1}{4n^2}\right]\delta_{\ell 0} + \frac{4}{27}\,\frac{n^2-1}{n^2}\,\delta_{\ell 1} ,$$

with Euler's constant γ and Psi function $\psi(z)$.

Values and uncertainties for B_{61} and B_{60} are listed in Tables 29.8 and 29.9, respectively. For the S-state values, the first number in parentheses for B_{60} is the state-dependent uncertainty $u_n(B_{60})$, while the second number in parentheses is the state-independent uncertainty $u_0(B_{60})$. It is worth noting that recently [32] computed an additional light-by-light correction to B_{61} for S-states. It only shifts this coefficient within its current uncertainty.

For S-states, the next term B_{72} is state independent, but its value is not known. The B_{71} coefficient is state dependent, although only the difference

$$\Delta B_{71}(n\mathrm{S}) = B_{71}(n\mathrm{S}) - B_{71}(1\mathrm{S}) = \pi\left(\frac{427}{36} - \frac{16}{3}\ln 2\right) \times \left[\frac{3}{4} - \frac{1}{n} + \frac{1}{4n^2} + \psi(n) + \gamma - \ln n\right] + \ldots$$

is known with a relative uncertainty $u_n(\Delta B_{71}) = 0.5\,\Delta B_{71}$. For our calculations, we use $B_{71}(1\mathrm{S}) = 0$.

As with the one-photon correction, the two-photon correction is multiplied by the reduced-mass factor $(m_{\rm r}/m_{\rm e})^3$, except the magnetic moment term proportional to $1/[\kappa(2\ell+1)]$ in B_{40}, which is multiplied by the factor $(m_{\rm r}/m_{\rm e})^2$, and the argument $(Z\alpha)^{-2}$ of the logarithms is replaced by $(m_{\rm e}/m_{\rm r})(Z\alpha)^{-2}$.

Table 29.6 Values of the function $G_{SE}(\alpha)$. Missing entries correspond to states for which no experimental measurements are available

n	$S_{1/2}$	$P_{1/2}$	$P_{3/2}$	$D_{3/2}$	$D_{5/2}$
1	−30.290240(20)				
2	−31.185150(90)	−0.97350(20)	−0.48650(20)		
3	−31.04770(90)				
4	−30.9120(40)	−1.1640(20)	−0.6090(20)		0.03163(22)
6	−30.711(47)				0.03417(26)
8	−30.606(47)			0.007940(90)	0.03484(22)
12				0.009130(90)	0.03512(22)

Table 29.7 Values of the function $G^{(1)}_{VP}(\alpha)$. No experimental data is available for missing entries. Zero values indicate that their contributions are negligibly small

n	$S_{1/2}$	$P_{1/2}$	$P_{3/2}$	$D_{3/2}$	$D_{5/2}$
1	−0.618724				
2	−0.808872	−0.064006	−0.014132		
3	−0.814530				
4	−0.806579	−0.080007	−0.017666		−0.000000
6	−0.791450				−0.000000
8	−0.781197			−0.000000	−0.000000
12				−0.000000	−0.000000

Table 29.8 Values of B_{61} used in the 2014 CODATA adjustment. Zero values indicate that their contributions are negligibly small

n	$S_{1/2}$	$P_{1/2}$	$P_{3/2}$	$D_{3/2}$	$D_{5/2}$
1	48.95859024(1)				
2	41.06216431(1)	0.157775547(1)	−0.092224453(1)		
3	38.904222(1)				
4	37.909514(1)	0.191192600(1)	−0.121307400(1)		0.0(0)
6	36.963391(1)				0.0(0)
8	36.504940(1)			0.0(0)	0.0(0)
12				0.0(0)	0.0(0)

Table 29.9 Values of B_{60} used in the 2014 CODATA adjustment. The uncertainties of B_{60} for S-states are explained in the text

n	$S_{1/2}$	$P_{1/2}$	$P_{3/2}$	$D_{3/2}$	$D_{5/2}$
1	−81.3(0.3)(19.7)				
2	−66.2(0.3)(19.7)	−1.6(3)	−1.7(3)		
3	−63.0(0.6)(19.7)				
4	−61.3(0.8)(19.7)	−2.1(3)	−2.2(3)		−0.005(2)
6	−59.3(0.8)(19.7)				−0.008(4)
8	−58.3(2.0)(19.7)			0.015(5)	−0.009(5)
12				0.014(7)	−0.010(7)

Three-Photon Corrections

The three-photon contribution in powers of $Z\alpha$ is

$$E^{(6)} = \left(\frac{\alpha}{\pi}\right)^3 \frac{(Z\alpha)^4}{n^3} m_e c^2 [C_{40} + C_{50}(Z\alpha) + C_{63}(Z\alpha)^2 \ln^3 (Z\alpha)^{-2} + \ldots] . \tag{29.53}$$

The leading term C_{40} is

$$C_{40} = \left[-\frac{568\, a_4}{9} + \frac{85\,\zeta(5)}{24} - \frac{121\,\pi^2\,\zeta(3)}{72} - \frac{84{,}071\,\zeta(3)}{2304} - \frac{71\,\ln^4 2}{27} - \frac{239\,\pi^2\,\ln^2 2}{135} + \frac{4787\,\pi^2\,\ln 2}{108} + \frac{1591\,\pi^4}{3240} - \frac{252{,}251\,\pi^2}{9720} + \frac{679{,}441}{93{,}312} \right] \delta_{\ell 0}$$

$$+ \left[-\frac{100\, a_4}{3} + \frac{215\,\zeta(5)}{24} - \frac{83\,\pi^2\,\zeta(3)}{72} - \frac{139\,\zeta(3)}{18} - \frac{25\,\ln^4 2}{18} + \frac{25\,\pi^2\,\ln^2 2}{18} + \frac{298\,\pi^2\,\ln 2}{9} + \frac{239\,\pi^4}{2160} - \frac{17{,}101\,\pi^2}{810} - \frac{28{,}259}{5184} \right] \frac{1-\delta_{\ell 0}}{\kappa(2\ell+1)} ,$$

where $a_4 = \sum_{n=1}^{\infty} 1/(2^n n^4) = 0.517479061\ldots$. Only partial results for C_{50} have been obtained [52, 53]. We use $C_{50} = 0$ with uncertainty $u_0(C_{50}) = 30\delta_{\ell 0}$. Finally, we use $C_{63} = 0$ and $u_n(C_{63}) = 1$ for this unknown coefficient. Recently, *Karshenboim* and *Ivanov* [54] determined several of these coefficients. The dominant effect of the finite mass of the nucleus is taken into account by multiplying the term proportional to $\delta_{\ell 0}$ by the reduced-mass factor $(m_r/m_e)^3$ and the term proportional to $1/[\kappa(2\ell+1)]$, the magnetic mo-

ment term, by the factor $(m_r/m_e)^2$. The contribution from four photons is expected to be negligible at the level of uncertainty of current interest.

Finite Nuclear Size

For S-states, the leading and next-order correction to the level shift due to the finite size of the nucleus is given by

$$E_{NS} = \mathcal{E}_{NS}\left\{1 - C_\eta \frac{m_r}{m_e}\frac{r_p}{\lambda\!\!\!^{-}_C} Z\alpha - \left[\ln\left(\frac{m_r}{m_e}\frac{r_p}{\lambda\!\!\!^{-}_C}\frac{Z\alpha}{n}\right) + \psi(n) + \gamma - \frac{(5n+9)(n-1)}{4n^2} - C_\theta\right](Z\alpha)^2\right\}, \tag{29.54}$$

where

$$\mathcal{E}_{NS} = \frac{2}{3}\left(\frac{m_r}{m_e}\right)^3 \frac{(Z\alpha)^2}{n^3}\, m_e c^2 \left(\frac{Z\alpha\, r_p}{\lambda\!\!\!^{-}_C}\right)^2 . \tag{29.55}$$

The coefficients C_η and C_θ are constants that depend on the charge distribution in the nucleus with values $C_\eta = 1.7(1)$ and $C_\theta = 0.47(4)$ for hydrogen.

For the $P_{1/2}$-states in hydrogen, the leading term is

$$E_{NS} = \mathcal{E}_{NS}\frac{(Z\alpha)^2(n^2-1)}{4n^2} . \tag{29.56}$$

For $P_{3/2}$-states and higher-ℓ-states, the nuclear-size contribution is negligible.

Nuclear-Size Correction to Self-Energy and Vacuum Polarization

For the lowest-order self-energy and vacuum polarization, the correction due to the finite size of the nucleus is

$$E_{NSE} = \left(4\ln 2 - \frac{23}{4}\right)\alpha(Z\alpha)\mathcal{E}_{NS}\delta_{\ell 0} , \tag{29.57}$$

and

$$E_{NVP} = \frac{3}{4}\alpha(Z\alpha)\mathcal{E}_{NS}\delta_{\ell 0} , \tag{29.58}$$

respectively.

Radiative-Recoil Corrections

Corrections for radiative-recoil effects are

$$E_{RR} = \frac{m_r^3}{m_e^2 m_p}\frac{\alpha(Z\alpha)^5}{\pi^2 n^3} m_e c^2 \delta_{\ell 0} \times \left[6\zeta(3) - 2\pi^2\ln 2 + \frac{35\pi^2}{36} - \frac{448}{27} + \frac{2}{3}\pi(Z\alpha)\ln^2(Z\alpha)^{-2} + d_{61}(Z\alpha)\ln(Z\alpha)^{-2} + \ldots\right]. \tag{29.59}$$

The uncertainty is controlled by the unknown coefficient d_{61} inside the square brackets. We use $d_{61} = 0$, $u_0(d_{61}) = 10$, and $u_n(d_{61}) = 1$. Corrections for higher-ℓ-states are negligible.

Nucleus Self-Energy

The nucleus self-energy correction for S-states of hydrogen is

$$E_{SEN} = \frac{4Z^2\alpha(Z\alpha)^4}{3\pi n^3}\frac{m_r^3}{m_p^2}c^2 \times \left[\ln\left(\frac{m_p}{m_r(Z\alpha)^2}\right)\delta_{\ell 0} - \ln k_0(n,\ell)\right], \tag{29.60}$$

with an uncertainty u_0 given by Eq. (29.60), with the factor in the square brackets replaced by 0.5. For higher-ℓ-states, the correction is negligible.

Total energy and uncertainty: the energy $E(nl_j)$ of a level is the sum of the contributions listed above. Uncertainties in the energy due to the fundamental constants, i.e., α, $m_e c^2$, etc., are taken into account through a least-squares adjustment. Uncertainties in the theory, i.e., from estimates of missing and uncomputed terms in the contributions, are taken into account with an energy correction $\delta(n\ell_j)$, with an uncertainty that is the rms sum of the uncertainties of the individual contributions

$$u^2[\delta(n\ell_j)] = \sum_i \left[u_{0i}^2(n\ell_j) + u_{ni}^2(n\ell_j)\right], \tag{29.61}$$

where $u_{0i}(n\ell_j)$ and $u_{ni}(n\ell_j)$ are the components of uncertainty u_0 and u_n of contribution i. Covariances of the δs are

$$u\left[\delta(n_1\ell_j), \delta(n_2\ell_j)\right] = \sum_i u_{0i}(n_2\ell_j)u_{0i}(n_1\ell_j) . \tag{29.62}$$

The corrections $\delta(n\ell_j)$, their uncertainties, and covariances are input data in the least-squares adjustment. A value for $\delta(n\ell_j)$ returned by the adjustment that lies outside its uncertainty indicates either an underestimate of the value of uncomputed terms in the contributions or a role for unexpected physics beyond QED. No such discrepancies have been found.

Acknowledgments The authors gratefully acknowledge helpful conversations with David Newell.

References

1. Sommerfeld, A.: Ann. Phys. **356**, 1 (1916)
2. International Bureau of Weights and Measures (BIPM). https://www.bipm.org/en/about-us/
3. Newell, D.B.: Phys. Today **67**, 35 (2014)
4. Eides, M.I., Grotch, H., Shelyuto, V.A.: Phys Rep **342**, 63 (2001)
5. Mohr, P.J., Newell, D.B., Taylor, B.N.: Rev. Mod. Phys. **88**, 035009 (2016)
6. Hanneke, D., Fogwell, S., Gabrielse, G.: Phys. Rev. Lett. **100**, 120801 (2008)
7. Wang, M., Audi, G., Kondev, F.G., Huang, W.J., Naimi, S., Xu, X.: Chin. Phys. **C**(41), 030003 (2017)

8. Feng, X.J., Zhang, J.T., Moldover, M.R., Yang, I., Plimmer, M.D., Lin, H.: Metrologia **54**, 339 (2017)
9. Laporta, S., Remiddi, E.: Phys. Lett. B. **301**, 440 (1993)
10. Laporta, S.: Nuovo Cimento **106**, 675 (1993)
11. Kurz, A., Liu, T., Marquard, P., Steinhauser, M.: Nucl. Phys. B. **879**, 1 (2014)
12. Aoyama, T., Hayakawa, M., Kinoshita, T., Nio, M.: Phys. Rev. D **91**, 033006 (2015)
13. Laporta, S.: Phys. Lett. B. **772**, 232 (2017)
14. Aoyama, T., Kinoshita, T., Nio, M.: Phys. Rev. D **97**, 036001 (2018)
15. Particle Data Group: Chin. Phys. C **38**, 090001 (2014)
16. Bouchendira, R., Cladé, P., Guellati-Khélifa, S., Nez, F., Biraben Phys, F.: Rev. Lett. **106**, 080801 (2011)
17. Parker, R.H., Yu, C., Zhong, W., Estey, B., Müller, H.: Science **360**, 191 (2018)
18. Audi, G., Wang, M., Wapstra, A.H., Kondev, F.G., MacCormick, M., Xu, X., Pfeiffer, B.: Chin. Phys. C **36**, 1287 (2012)
19. Wang, M., Audi, G., Wapstra, A.H., Kondev, F.G., MacCormick, M., Xu, X., Pfeiffer, B.: Chin. Phys. C **36**, 1603 (2012)
20. Huang, W.J., Audi, G., Wang, M., Kondev, F.G., Naimi, S., Xu, X.: Chin. Phys. C **41**, 030002 (2017)
21. Sturm, S., Köhler, F., Zatorski, J., Wagner, A., Harman, Z., Werth, G., Quint, W., Keitel, C.H., Blaum, K.: Nature **506**, 467 (2014)
22. Köhler, F., Sturm, S., Kracke, A., Werth, G., Quint, W., Blaum, K.J.: Phys. B **48**, 144032 (2015)
23. Sturm, S., Wagner, A., Kretzschmar, M., Quint, W., Werth, G., Blaum, K.: Phys. Rev. A **87**, 030501 (2013)
24. Sturm, S., Wagner, A., Kretzschmar, M., Quint, W., Werth, G., Blaum, K. (2015), private communication.
25. Breit, G.: Nature **122**, 649 (1928)
26. Yerokhin, V.A., Harman, Z.: Phys. Rev. A **95**, 060501 (2017)
27. Beier, T., Lindgren, I., Persson, H., Salomonson, S., Sunnergren, P., Häffner, H., Hermanspahn, N.: Phys. Rev. A **62**, 032510 (2000)
28. Pachucki, K., Czarnecki, A., Jentschura, U.D., Yerokhin, V.A.: Phys. Rev. A **72**, 022108 (2005)
29. Jentschura, U.D., Czarnecki, A., Pachucki, K., Yerokhin, V.A.: Int. J. Mass. Spectrom. **251**, 102 (2006)
30. Jentschura, U.D.: Phys. Rev. A **79**, 044501 (2009)
31. Yerokhin, V.A., Harman, Z.: Phys. Rev. A **88**, 042502 (2013)
32. Czarnecki, A., Szafron, R.: Phys. Rev. A **94**, 060501 (2016)
33. Eides, M.I., Grotch, H.: Ann. Phys. **260**, 191 (1997)
34. Czarnecki, A., Melnikov, K., Yelkhovsky, A.: Phys. Rev. A **63**, 012509 (2001)
35. Shabaev, V.M., Yerokhin, V.A.: Phys. Rev. Lett. **88**, 091801 (2002)
36. Karshenboim, S.G.: Phys. Lett. A. **266**, 380 (2000)
37. Glazov, D.A., Shabaev, V.M.: Phys. Lett. A. **297**, 408 (2002)
38. Angeli, I.: Data Tables. At. Data. Nucl. **87**, 185 (2004)
39. Parthey, C.G., Matveev, A., Alnis, J., Bernhardt, B., Beyer, A., Holzwarth, R., Maistrou, A., Pohl, R., Predehl, K., Udem, T.: Phys. Rev. Lett. **107**, 203001 (2011)
40. Matveev, A., Parthey, C.G., Predehl, K., Alnis, J., Beyer, A., Holzwarth, R., Udem, T., Wilken, T., Kolachevsky, N., Abgrall, M.: Phys. Rev. Lett. **110**, 230801 (2013)
41. T. Udem (2014), private communication.
42. Lundeen, S.R., Pipkin, F.M.: Metrologia **22**, 9 (1986)
43. Newton, G., Andrews, D.A., Unsworth, P.J.: Philos. Trans. R. Soc. Lond. Ser. A **290**, 373 (1979)
44. Beyer, A., Maisenbacher, L., Matveev, A., Pohl, R., Khabarova, K., Grinin, A., Lamour, T., Yost, D.C., Hänsch, T.W., Kolachevsky, N.: Science **358**, 79 (2017)
45. Fleurbaey, H., Galtier, S., Thomas, S., Bonnaud, M., Julien, L., Biraben, F., Nez, F., Abgrall, M., Guéna, J.: arXiv, 1801:0881 (2018)
46. Barker, W.A., Glover, F.N.: Phys. Rev. **99**, 317 (1955)
47. Sapirstein, J.R., Yennie, D.R.: chap. 12. In: Kinoshita, T. (ed.) in *Quantum Electrodynamics*, pp. 560–672. World Scientific, Singapore (1990)
48. Erickson, G.W.: J. Phys. Chem. Ref. Data **6**, 831 (1977)
49. Yerokhin, V.A., Shabaev, V.M.: Phys. Rev. Lett. **115**, 233002 (2015)
50. Yerokhin, V.A., Shabaev, V.: Phys. Rev. A **93**, 062514 (2016)
51. Mohr, P.J., Taylor, B.N., Newell, D.B.: Rev. Mod. Phys. **84**, 1527 (2012)
52. Eides, M.I., Shelyuto, V.A.: Phys. Rev. A **70**, 022506 (2004)
53. Eides, M.I., Shelyuto, V.A.: Can. J. Phys. **85**, 509 (2007)
54. Karshenboim, S.G., Ivanov, V.G.: Phys. Rev. A **98**, 022522 (2018)

Eite Tiesinga Dr Eite Tiesinga received his PhD from Eindhoven University of Technology in The Netherlands in 1993. He works at the National Institute of Standards and Technology and the University of Maryland in the US. His research focuses on developing clocks and sensors using laser-cooled atoms. He maintains a web-based database of fundamental constants, an initiative by the Committee on Data of the International Science Council (CODATA).

Peter Mohr Peter Mohr received his PhD from the University of California at Berkeley (1973) and spent some years at the Lawrence Berkeley Laboratory (1973–1978), Yale University (1978–1985), the National Science Foundation (1985–1987), and the National Bureau of Standards/National Institute of Standards and Technology (from 1987). He held the Chair of the CODATA Task Group on Fundamental Constants (1999–2006) and was Chair of the Precision Measurement and Fundamental Constants Topical Group of the American Physical Society (2000–2001).